SPE 95656

A Comprehensive Model of Temperature Behavior in a Horizontal Well

K.Yoshioka, D. Zhu, and A.D. Hill, Texas A&M U., and P. Dawkrajai and L.W. Lake, U. of Texas at Austin

This paper was prepared for presentation at the 2005 SPE Annual Technical Conference and Exhibition held in Dallas, Texas, U.S.A., 9 – 12 October 2005.

Abstract

Use of distributed temperature sensors is becoming increasingly common for monitoring producing sections of horizontal wells through a real-time measurement of a temperature profile. This information can potentially be inverted to infer the types and amounts of fluid entering along the wellbore. This information is essential for reservoir management to identify excessive water or gas influx, to guide the action of sliding sleeves or other downhole flow control devices, and to decide if reservoir stimulation is needed in a particular horizontal section.

The inferences described above require a model to translate temperature information into flow information. This paper presents a model for predicting the temperature profile in a nominally horizontal well during normal production (steady-state flow). A forward model of the temperature profile caused by given flow conditions can be the basis of the inverse model needed to determine flow profiles

Prediction of the wellbore temperature profile requires models of all of the often-subtle thermal effects occurring in the reservoir and in the wellbore itself. For the reservoir temperature model, we couple mass and energy balances of fluid flow in a permeable media in a box-shaped homogeneous reservoir with a wellbore temperature model using a multisegment technique. Similarly for the wellbore, we couple mass, momentum, and energy balances to model pressure and temperature behavior. The models presented in this paper account for Joule-Thomson effects, and convective and conductive heat transfer. The primary results of the model are estimates of the extent of temperature change from geothermal temperature during flow. Results show that temperature changes of a few degrees are possible; temperature changes of this magnitude are certainly detectable with current technology. A second result is a demonstration of the inference of single phase and multiphase flow profiles from a synthetic case. Sensitivity studies with the model illustrate the flow conditions that cause measurable temperature changes or anomalies that could be recognized in an analysis of distributed temperature measurements.

Introduction

Temperature logs have been used successfully in vertical wells to locate gas entries, detect casing leaks, evaluate cement placement, and estimate inflow profiles[1]. Recently, interpretations of temperature profiles in horizontal wells are reported to be useful to identify types of fluid flowing to a wellbore[2-4]. The unwanted fluid is subsequently isolated by means of intelligent well technology. These benefits and the advancement of temperature measurements in horizontal wells during production have motivated this work.

Downhole temperature measurements have been continuously improved in term of resolution, accuracy and reliability. Current fiber optic measurements can provide a near-continuous profile of distributed temperature with resolution less than 0.1 ^{o}C, over a distance of several kilometers, with a spatial resolution of one meter, and with a measurement time of typically a few minutes.

To identify the causes of a measured temperature variation, we must have reservoir and wellbore temperature models to relate a measured temperature to the inflow profile of the well. These models must account for all the subtle thermal energy effects including Joule-Thomson expansion, viscous dissipative heating, and thermal conduction.

In our previous work[5], we calculated temperature profiles in horizontal wells in which the inflowing fluid temperature depended only on depth. To relax this assumption, here the energy balance in permeable media has been coupled with wellbore temperature and pressure equations. The reservoir and wellbore temperatures are intimately coupled, and this coupling must be included in the model of the process. For example, consider a well that is producing gas near the toe of the well and oil along the rest of the well. Along the gas inflow section, the temperature will be lower than geothermal temperature because of Joule-Thomson cooling. When this relatively cool fluid reaches the oil producing sections of the wellbore, both heat conduction and convective transport will increase the wellbore temperature. The wellbore and reservoir systems must be coupled to model such effects.

Fig. 1 shows the geometry of a multi-segmented reservoir containing a horizontal wellbore that is to be discussed throughout this study. The objective of this coupled model is to provide a basis for estimating the size of the temperature change away from geothermal temperature, and to identify

temperature anomalies that can be interpreted to define phase inflow profiles.

Physical Description of Coupled Model

The coupled model consists of a reservoir flow model, wherein conservation of mass and energy is solved along with Darcy's Law, and a wellbore model that solves conservation of mass, energy and momentum equations.

We consider a horizontal well fully penetrated through a box-shaped homogeneous reservoir as shown in Fig. 2. With no-flow lateral boundaries, flow in the reservoir is only in the y and z directions; flow in the horizontal wellbore is in the x-direction. The assumptions for this coupled model are the following:

1) Steady-state flow: For continuous well flow, changes in the well rate are much slower than the response time of any sensor; hence, we can neglect time derivatives in our treatment. We use the steady-state model of Butler[6] or Furui et al.[7] to describe the pressure profile in the reservoir (these models are virtually identical, though derived in different ways.)

2) Isolated reservoir segments: Each segment of the reservoir is idealized to be isolated from each other. There is no flow in the x-direction within the reservoir.

3) Single-phase reservoir flow: Each reservoir segment produces a single-phase fluid. Multiphase flow occurs only in the wellbore as a result of the combination of single phase flows of different phases from the reservoir segments.

Reservoir flow equations

The model couples an energy and component mass balance to calculate the pressure drops and the resulting temperature distribution caused by flowing fluid at steady -state.

The fluid flow is governed by a mass balance

$$\nabla\cdot(\rho\mathbf{u})=0 \tag{1}$$

where

$$\mathbf{u}=-\frac{\vec{\vec{\mathbf{k}}}}{\mu}\cdot(\nabla p+\rho\mathbf{g}) \tag{2}$$

Equation 2 is a form of Darcy's Law. A familiar form of the mass balance is a combination of Eqs. 2 and 3 that is expressed in term of pressure. For isotropic permeable media with negligible gravity, these equations become

$$\nabla^2 p+c(\nabla p)^2=0 \tag{3}$$

where c is the compressibility of the fluid. For slightly compressible fluid, the term $c(\nabla p)^2$ is commonly dropped.

The temperature behavior of the fluid is governed by an energy balance, which is given as[8]

$$\rho C_p\mathbf{v}\cdot\nabla T-\beta T\mathbf{v}\cdot\nabla p-\nabla\cdot\left(\vec{\vec{\mathbf{K}}}_T\cdot\nabla T\right)-(-\vec{\vec{\boldsymbol{\tau}}}:\nabla\mathbf{v})=0 \tag{4}$$

where C_p is the heat capacity of the fluid. β is the thermal expansion coefficient defined as

$$\beta=\frac{1}{\hat{V}}\left(\frac{\partial\hat{V}}{\partial T}\right)_p \tag{5}$$

The term $\left(-\vec{\vec{\boldsymbol{\tau}}}:\nabla\mathbf{v}\right)$ represents heating by viscous dissipation, the degradation of mechanical energy into thermal energy because of friction. This term is commonly replaced by $(-\mathbf{u}\cdot\nabla p)$ in flow through permeable media[9]. The thermal conductivity, $\mathbf{K}_T$ combines both fluid and matrix conductivity. Empirical expressions for $\mathbf{K}_T$ can be found in the literature[10]. For a fluid-filled consolidated sandstone, an example expression is

$$K_T=K_d\left\{1+0.299\left[\left(\frac{K_{fl}}{K_a}\right)^{0.33}-1\right]+4.57\left[\frac{\phi K_{fl}}{(1-\phi)K_d}\right]^{0.482}\left[\frac{\rho}{\rho_s}\right]^{-4.30}\right\} \tag{6}$$

where the subscripts t, f, a, and d refer to total, fluid, air and dry respectively. $\mathbf{K}_T$ depends weakly on temperature and is treated as a constant here. The energy equation now becomes

$$\rho C_p\mathbf{u}\cdot\nabla T-\beta T\mathbf{u}\cdot\nabla p-\nabla\cdot\left(\vec{\vec{\mathbf{K}}}_T\cdot\nabla T\right)+\mathbf{u}\cdot\nabla p=0 \tag{7}$$

The first term in Eq. 7 is the thermal energy transported by convection. The second term is thermal energy change caused by fluid expansion. The third term is thermal energy transported by heat conduction, and the last term represents the viscous dissipative heating.

For linear flow Eq. 7 can be solved analytically to yield

$$T=L_1 e^{m_+ y}+L_2 e^{m_- y}+\frac{1}{\beta} \tag{8}$$

The radial flow solution is

$$T=R_1 r^{n_+}+R_2 r^{n_-}+\frac{1}{\beta} \tag{9}$$

where y is the linear coordinate and r is the radial coordinate. The solution procedure is presented in Appendix A and all parameters are defined there.

The temperature profiles perpendicular to the wellbore of fluid flowing into a wellbore for various inflow rates, permeabilities and fluid types are shown in Figs. 3-5. The input parameters used are in Table 1.

Fig. 3 shows how the temperature in the reservoir varies with different oil flow rates. As flow rate increases, the temperature change increases because larger frictional pressure drop leads to a greater Joule-Thomson effect. Fig. 4 shows the effect of permeability on temperature distribution with a fixed flow rate. The inflow temperature decreases as permeability increases because less pressure drop caused by higher permeability leads to a smaller Joule-Thomson effect. Fig. 5 presents the reservoir temperature profiles with different fluids. It is obvious that the temperature of gas is substantially lower than the geothermal temperature because of Joule-Thomson cooling. The temperature of water is slightly lower than for oil because water has a greater heat capacity.

Coupled wellbore model

The wellbore will have mass and heat transfer from the reservoir (in the r-direction) and flow along the wellbore axis, in the x-direction. We derived the steady-state conservation equations for the wellbore region averaging any variation in temperature or pressure in the r-direction over a volume element of the wellbore.

The reservoir and wellbore model are coupled to generate the temperature and pressure field in the system. As mentioned before, the flow geometry inside the reservoir is assumed to be a sequence of 1D linear and radial flow as illustrated in Fig. 2. The reservoir is divided into several segments that only communicate through the wellbore. Each segment of the reservoir can produce different fluid into the wellbore (oil, water or gas).

Multiphase flow can occur inside the wellbore. The multiphase mass balance equation for each phase[5] is

$$\frac{d(\rho_i v_i y_i)}{dx} = \frac{2\gamma}{R}\rho_{i,I} v_{i,I} \tag{10}$$

where i is an index on the phases and y_i is the holdup of phase i. γ is an average open pipe ratio over some finite length defined as,

$$\gamma = \frac{\text{Open pipe surface area}}{\text{Pipe surface area}} \tag{11}$$

Inflow rate for each segment is calculated as

$$\int_{\Delta x} 2\pi R\gamma v_{i,I} y_{i,I}\, dx = J_i(p_R - p) \tag{12}$$

The productivity index J_i for a slice of reservoir is given as[6]

$$J_i = \frac{2k_i h\Delta x}{\mu_i}\left\{\frac{Y}{2} + \frac{h}{\pi}\ln\left(\frac{h}{2\pi R}\right)\right\}^{-1} \tag{13}$$

Since every segment of the reservoir is in single-phase flow, J_i will be zero where phase i is not produced.

The energy balance equation[5] is given by

$$\frac{dT}{dx} = \frac{2U_I}{R(\rho v C_p)_T}(T_I - T) + \frac{(\rho v C_p K_{JT})_T}{(\rho v C_p)_T}\frac{dp}{dx} + \frac{(\rho v)_T}{(\rho v C_p)_T} g\sin\theta \tag{14}$$

where

$$(\rho v)_T = \sum_i \rho_i v_i y_i \tag{15}$$

$$(\rho v C_p)_T = \sum_i \rho_i v_i y_i C_{p,i} \tag{16}$$

$$(\rho v C_p K_{JT})_T = \sum_i \rho_i v_i y_i C_{p,i} K_{JT,i} \tag{17}$$

U_I is a combined convection and conduction overall heat transfer coefficient, defined here as

$$U_I = \gamma(\rho v C_p)_{T,I} + (1-\gamma)U \tag{18}$$

The first term is the resistance to heat transport because of convected fluid and the second term is a resistance to conduction. The estimation of U is discussed in Appendix B. This combined overall heat transfer coefficient is multiplied by the difference between the reservoir temperature just outside the completion and wellbore temperature and by the outside surface area of the wellbore to arrive at an expression for energy flux. If the heat transfer coefficient is very large, the wellbore and the reservoir inflow temperature approach the same temperature.

The second term of Eq. 14 represents the Joule-Thomson effect, which depends on the pressure gradient along the wellbore. The pressure gradient is calculated from the multiphase momentum balance. We treat the fluid in the wellbore as a homogeneous mixture of two phases. For oil-water two phase flow we use the mixture viscosity property[11] that includes phase inversion point[12] For oil-gas two phase flow, we apply a drift-flux model corrected for wall influx[13]. A gas-liquid slip velocity correlation[14] is applied for estimation of gas holdup. Since the coupled equations are nonlinear, we solved them numerically applying successive substitution[15].

Results and Discussion

This section shows some example cases using the coupled model. We are interested in determining the conditions for which measureable temperature changes occur along a horizontal wellbore, so we focus on how much temperature change is possible under specifed conditions. We also looked for conditions that caused anomalies in the pressure or temperature profiles caused by the inflow of different fluids.

We consider two kinds of wells; one with a small diameter and the other large, and both are completed as cased, perforated wells. The details are shown in Table 2. Oil, gas and water are the produced fluids. The average reservoir pressure is 4000 psia, except for the single-phase gas reservoir for which it is 2000 psia. The reservoir geometry described in Table 1 is considered. The physical properties of the fluids are listed in Table 3.

Possible temperature changes in single-phase production

To evaluate the temperature changes possible along the wellbore in a single-phas production system, we studied two extreme cases; small and large production scenarios with small or large well diameter. These cases should bracket the possible temperature changes in actual wells.

Fig. 6 displays the flow rate profile and pressure change from the toe pressure for flow through a small diameter well. With a total flow rate of about 5300 b/d, the total pressure drop in the 2000 ft. long wellbore is only about 50 psi; at a very high rate of almost 20,000 b/d, the wellbore pressure drop is over 600 psi. The corresponding temperature change profiles, the temperature at any location along the well minus the temperature at the toe along the wellbore, are shown in Fig. 7. For the lower flow rate case, the temperature changes only 0.5 ^{o}F from the toe to the heel of the well. In the large production rate case, the temperature deviation is substantial (6.4 ^{o}F). This case, a high flow rate in a small diameter well,

illustrates the largest temperature change that can be expected in a horizontal single-phase oil production well.

Table 4 summarizes results from several other cases. The profiles for each are similar to those shown in Figs. 6 and 7. In these calculations the temperature changes for low production rates with the larger diameter wellbore for both oil (maximum change of 0.06 ^{o}F) and gas production (0.02 ^{o}F) cases were small. However, if the production rate is large, the temperature change would be measurable. Even though the pressure change along a well producing gas is small, the temperature change of gas is more sensitive to the production rate.

Pressure and temperature profiles with various well trajectories

Horizontal wells are often not perfectly horizontal, with varying inclination angles along the well trajectory. Deviations of the well trajectory may alter the temperature and pressure distributions along the wellbore from the profiles of a perfectly horizontal wellbore.

The geothermal temperature of the formation monotonically increases with depth, so that in an upwards flow, the wellbore fluids will encounter cooler formation temperatures as they move up the wellbore, while with a downwards trajectory, the wellbore stream will contact warmer surroundings. To study these effects, we considered the upward and downward well trajectories shown in Figs. 8 and 9. These results are compared with the horizontal small-diameter case that has a uniform inflow (5 bbl/day/ft for oil, 25 MCF/day/ft for gas).

For oil flow, the pressure loss will be larger in upward flow compared to horizontal flow because of the decreasing hydrostatic pressure drop. Fig. 10 shows the pressure change from the toe pressure (wellbore Δp) for upward trajectories, at a uniform angle ($+5^{o}$) and at varying inclinations ($+5^{o}$ to $+2^{o}$). Since upward with $+5^{o}$ case results in a larger elevation change, the pressure drop is higher and formation temperature will be cooler because of the geothermal temperature effect. Fig. 11 plots the temperature deviations from the toe temperature. Both plots show more cooling than in the horizontal case but there is little difference between the two inclination cases. There are two factors that affect the temperature profile in this process; one is a pressure dependence of the Joule-Thomson coefficient and the other is a cooler surrounding temperature. At lower pressures, the Joule-Thomson coefficient of a liquid is larger. The first factor tends to increase the temperature when the wellbore pressure becomes low (high pressure drop in the wellbore) and the other factor tends to decrease it. Therefore, uniform angle case ($+5^{o}$) experiences higher pressure drop and cooler surrounding temperature, but has a larger Joule-Thomson coefficient.

Similar but opposite effects can be observed in downwards cases. Compared to the horizontal case the downward wellbore pressure drop is less (Fig. 12) and the temperature increase is smaller (Fig 13). Again there is very little difference between the -5^{o} inclination and -5^{o} to -2^{o} inclinations. However, we clearly see the difference between the horizontal and $\pm 5^{o}$ inclinations. With $\pm 5^{o}$ inclinations, geothermal gradient effects are more significant than Joule-Thomson effects.

Next, we present the gas production cases. Fig. 14 shows wellbore pressure drop for two kinds of upward trajectories. The more upward the inclination, the more the pressure drops. Since the Joule-Thomson coefficient of gas will be smaller at lower pressures, higher pressure drops causes more Joule-Thomson cooling. Therefore, upward gas flow is cooled by both the temperature change in the formation and pressure drop. Temperature deviations are shown in Fig. 15. The temperature change is significant even though the wellbore pressure drop is small. Similarly, downward examples are shown in Fig. 16 and Fig. 17. We can find where the well changes inclination from the temperature profile.

Water and gas production effects

As a last example, we present cases in which gas or water are produced from some zones while oil is produced from others. Fig. 5 shows that each phase will enter the wellbore with a different temperature. Water enters at a lower temperature than oil because of its larger heat capacity; gas enters at a lower temperature because of Joule-Thomson cooling.

We first consider water entries from different positions along a horizontal wellbore. The water entry zone is 400 feet long, and the rest of the well has oil inflow with a constant productivity index. For the large diameter well with the wellbore pressure at the heel set at 3300 psia, we examine cases that have water entry at the toe, in the middle, and at the heel of the well. Water holdup profiles (Fig. 18) show the water holdup increasing along the water entry zones. Total production for each case is about 10000 bbl/d and water cut is about 0.2. Since the pressure profiles are identical for each case, we only show the temperature deviation (temperature at any location minus the temperature at the toe) profiles (Fig. 19). There are clear discontinuities in these profiles; where the water entry starts and ends is readily identifiable. This anomalous temperature behavior is caused primarily by differences in Joule-Thomson effects in the reservoir flow near the well.

To explain this complex temperature behavior, consider the case where water is being produced in the middle of the well, from the interval from 800 to 1200 feet from the heel of the well. Beginning at the toe of the well, oil is being produced over the interval from 1200 feet to 2000 feet from the heel. According to Fig. 5, with a far field reservoir temperature of 180 ^{o}F, this oil enters the wellbore at a temperature of about 183 ^{o}F. The water being produced experiences less Joule-Thomson heating and arrives at the wellbore at about 181 ^{o}F. Since the inflow and wellbore fluid interact as described in Appendix A, these inflow temperatures will be damped in the calculation. Thus, the temperature in the well begins to drop at the start of the water entry zone and continues to decrease across this entire zone. At the end of the water zone (800 feet from the heel), production into the well of relatively warm oil reverses this trend and the wellbore temperature increases gradually all the way to the heel. Thus, for this scenario, the water zone is clearly identifiable as the region over which the welbore temperature is decreasing, moving towards the heel. The temperature profiles for the other cases shown in Fig. 19 can be interpreted in a similar manner.

For the oil and gas production case, we illustrate the behavior that will occur with gas zones of different lengths. In

these cases, the gas zone begins at the heel of the well and extends 400, 1000, or 1600 feet along the wellbore. The remainder of the 2000 ft long well is receiving oil production. The pressure at the heel was set to 3200 psi for this example. The gas holdup and pressure change profiles are shown in Figs. 20 and 21. Since the pressure drops inside the wellbore are small, oil and gas inflow rates are almost uniform in each fluid production zones. Oil inflow rate is about 5.7 bbl/d/ft and gas is about 6.3 MSCF/d/ft, respectively. Figs. 22-24 show the wellbore temperature and inflow temperature deviation profiles. Since gas flow results in a lower temperature than geothermal temperature, the difference from oil temperature is significant. As the gas rate increases, the temperature deviation increases (Fig. 23). In the case with gas being produced in the 400 foot interval at the heel of the well, the temperature gain and loss are canceled out and we see small changes (-0.1 ^{o}F). Gas production should decrease the temperature; therefore this type of temperature profile with gas production tells us that gas enters near the heel. In other cases it is obvious where gas production occurs. Temperature deviations are very high.

Summary and Conclusions

We have derived the governing equations that describe reservoir fluid flow and heat transfer, and solved them analytically in one-dimensional (1D) flow. Results from the 1D analytical reservoir solution indicate that the inflow temperature can change from the geothermal temperature by a few degrees. The size of this change depends on the types of fluids flowing and especially on the well's producing rate. Inasmuch as we must account for the heat transfer from wellbore to formation, we have coupled wellbore and reservoir equations and solved them numerically.

Based on the coupled model predictions we see little changes on the temperature profiles if the liquid flow rate is quite small or if the pressure drop along the well is small for gas production. We found that temperature and pressure profiles are sensitive to the well trajectories, meaning that an accurate well survey is needed to interpret temperature and pressure profiles when significant elevation changes occur.. Perhaps most significantly, the temperature profile shows strong discontinuity in its slope when we pass between zones that are producing different fluids. Where the production of one fluid starts and another ends is clearly observed.

The originally stated goal of this work was to find the conditions under which continuous temperature measurements in a horizontal well can be used to quantitatively infer fluid inflow. Our results suggest that this approach will be most successful (that is, temperature changes will be detectable) in oil wells flowing at a high rate, in gas wells, or in wells with a small diameter. The effect of an inclined wellbore can cause the temperature change to be larger (compared to a horizontal well) if the well is inclined downward. Inclination upward can also suppress the temperature change. Perhaps the most significant finding is that readily detectable discontinuities in the slope of a temperature profile appear to clearly indicate where the entry of one fluid begins and another ends.

Nomenclature

C_p	specific heat capacity
e	total energy flux
f	friction factor
g	gravity acceleration
h	reservoir thickness
J	productivity index
k	permeability
K	thermal conductivity
K_T	total thermal conductivity of rock and fluid
L	length of well
p	pressure,
Pr	Prandtl number
p_R	reservoir pressure
q	volumetric flow rate, heat flux
Re	Reynolds number
Q	heat transfer rate per unit length of wellbore
R	inner wellradius
T	temperature
T_I	inflow temperature of fluid entering a wellbore
T_o	temperature at external boundary of reservoir
$\mathbf{u}$	Darcy velocity vector
U	overall heat transfer coefficient
v	fluid velocity
$\hat{V}$	specific volume
w	mass flow rate
Y	length of reservoir
α	heat transfer coefficient
β	thermal expansion coefficient
γ	pipe opened ratio
μ	viscosity
ρ	density
ϕ	porosity
θ	angle from horizontal
$\boldsymbol{\tau}$	stress shear tensor

Subscripts

a	air
b	bulk
c	casing
d	dry rock
cem	cement
fl	fluid
g	gas
I	inflow
i	phase
l	liquid
o	oil
s	solid part of rock

Acknowledgements

The authors are grateful for the financial support of the U.S. Department of Energy through Contract Number DE-FC26-03NT15402. Larry W. Lake hold the W.A. (Monty) Moncrief Chair at The University of Texas. A.D. Hill holds the Robert L. Whiting Endowed Chair at Texas A&M University.

References

1. Hill, A.D.: *Production Logging -Theoretical and Interpretive Elements*, Society of Petroleum Engineers Inc., Richardson, TX, 1990.
2. Brown, G., Storer, D., McAllister, K., Al-Asimi, M., and Raghavan, K. : "Monitoring Horizontal Producers and Injectors During Cleanup and Production Using Fiber-Optic-Distributed Temperature Measurements," paper SPE 84379 presented at the SPE Annual Technical Conference and Exhibition, Denver, CO, 5-8 October, 2003.
3. Tolan, M., Boyle, M., and Williams, G. : "The Use of Fiber-Optic Distributed Temperature Sensing and Remote Hydraulically Operated Interval Control Valves for the Management of Water Production in the Douglas Field," paper SPE 71676 presented at the 2001 SPE Annual Technical Conference and Exhibition, New Orleans, LA, 30 September-3 October, 2001.
4. Foucault, H., Poilleux, D., Djurisic, A., Slikas, M., Strand, J., and Silva, R.: "A Successful Experience for Fiber Optic and Water Shut Off on Horizontal Wells with Slotted Liner Completion in an Extra Heavy Oil Field," paper SPE 89405 presented at the 2004 SPE/DOE Fourteenth Symposium on Improved Oil Recovery, Tulsa, OK, 17-21 April, 2004.
5. Yoshioka, K., Zhu, D., Hill, A.D., and Lake, L.W.: "Interpretation of Temperature and Pressure Profiles Measured in Multilateral Wells Equipped with Intelligent Completions," paper SPE 94097 presented at the 14th Europec Biennial Conference, Madrid, Spain, 13-16 June, 2005.
6. Butler, R.M. ; *Horizontal Wells for the Recovery of Oil, Gas, and Bitumen*, The Petroleum Society of the Canadian Institute of Mining, Metallurgy and Petroleum, Calgary, Canada, 1994.
7. Furui, K., Zhu, D., and Hill, A.D.: "A Rigorous Formation Damage Skin Factor and Reservoir Inflow Model for a Horizontal Well," SPE Production and Facilities, pp. 151-157, August 2003.
8. Bird, R. B., Stewart, W.E., and Lightfoot, E.N.; *Transport Phenomena*, second edition, John Wiley and Sons, New York, NY, 2002.
9. Al-Hadhrami, A.K., Elliott, L., and Ingham, D.B.,: "A New Model for Viscous Dissipation in Porous Media Across a Range of Permeability Values," *Transport in Porous Media 53*, Netherlands, 2003.
10. Lake, L. W.: *Enhanced Oil Recovery*, Prentice Hall, Saddle River, NJ, 1989.
11. Brinkman, H. C.: "The Viscosity of Concentrated Suspensions and Solutions," J. Chem. Hydrodynamics (1952) 571.
12. Decarre, S. and Fabre, J.: "Phase Inversion Prediction Study," Jounal of L'Institut Francais du Petrole (1997) 415-424.
13. Ouyang, L.-B. and Aziz, K.: "A homogeneous model for gas-liquid flow in horizontal wells," *Journal of Petroleum Science and Engineering* (2000) 119-128.
14. Shi, H., Holmes, J.A., Diaz, L.R. and Aziz, K.: "Drift-Flux Parameters for Three-Phase Steady-State Flow in Wellbores," paper SPE 89836 presented at the SPE Annual Technical Conference and Exhibition, Houston, TX, 2004.
15. Reddy, J.N. and Gartling, D.K. : *The Finite Element Method in Heat Transfer and Fluid Dynamics*, second edition, CRC Press, Boca Raton, 2001
16. Mills, A. F.: *Heat Transfer*, second edition, Prentice Hall, Saddle River, NJ, 1999
17. Kim, D., and Ghajar, A. J.: "Heat transfer measurements and correlations for air-water flow of different flow patterns in a horizontal pipe," *Experimental Thermal and Fluid Science* (2002) 659-676.
18. McCain, W. D., Jr.: *The Properties of Petroleum Fluids*, second edition, PennWell Publishing Company, Tulsa, Oklahoma, 1990.
19. Economides, M.J., Hill, A.D., and Ehlig-Economides, C.: *Petroleum Production Systems*, Prentice Hall Inc., New Jersey 1994.

Appendix A: Inflow Temperature Model for Slightly Compressible Fluid

The object of this Appendix is to derive and solve analytically the equations for reservoir flow. The pressure relationship is described by Darcy's law as:

$$u_y = -\frac{k}{\mu}\frac{dp}{dy} \tag{A-1}$$

In terms of the volumetric flow rate this becomes.

$$\frac{q}{2Lh} = -\frac{k}{\mu}\frac{dp}{dy} \tag{A-2}$$

In a one-dimensional Cartesian coordinate (y-direction), the energy balance becomes

$$\rho C_p u_y \frac{dT}{dy} - \beta T u_y \frac{dp}{dy} + u_y \frac{dp}{dy} - K_T \frac{d^2T}{dy^2} = 0 \tag{A-3}$$

Substituting Eq. A-2 into Eq.A-3 and rearranging give

$$\frac{d^2T}{dy^2} - \frac{\rho C_p}{K_T}\left(\frac{q}{2hL}\right)\frac{dT}{dy} - \frac{\beta\mu}{kK_T}\left(\frac{q}{2hL}\right)^2 T + \frac{\mu}{kK_T}\left(\frac{q}{2hL}\right)^2 = 0 \tag{A-4}$$

Solving the second order ordinary differential equation gives

$$T = L_1 e^{m_+ y} + L_2 e^{m_- y} + \frac{1}{\beta} \tag{A-5}$$

where

$$m_{\pm} = \frac{q}{4hL}\left[\frac{\rho C_p}{K_T} \pm \sqrt{\left(\frac{\rho C_p}{K_T}\right)^2 + \frac{4\beta\mu}{kK_T}}\right] \quad \text{(A-6)}$$

L_1 and L_2 are integration constants to be determined by boundary conditions.

For the radial flow portion consider a steady-state radial flow in a homogeneous reservoir with length, L, and outer radius of $h/2$. Similarly, from Darcy's Law

$$\frac{q}{2\pi rL} = -\frac{k}{\mu}\frac{dp}{dr} \quad \text{(A-7)}$$

In radial coordinates the energy balance becomes

$$\rho C_p\, u_r \frac{dT}{dr} - \beta T\, u_r \frac{dp}{dr} + u_r \frac{dp}{dr} - K_T \frac{1}{r}\frac{d}{dr}\left(r\frac{dT}{dr}\right) = 0 \quad \text{(A-8)}$$

Substituting equation A-7 into Eq. A-8 gives

$$-\frac{2\pi L\, K_{Tt}}{q} r^2 \frac{d^2T}{dr^2} + \left(\rho C_p - \frac{2\pi L\, K_T}{q}\right) r\frac{dT}{dr} + \frac{\mu q \beta T}{2\pi kL} - \frac{\mu q}{2\pi kL} = 0 \quad \text{(A-9)}$$

Solution to this second order differential equation is given by

$$T = R_1 r^{n_+} + R_2 r^{n_-} + \frac{1}{\beta} \quad \text{(A-10)}$$

where

$$n_{\pm} = \frac{q}{4\pi L}\left[\frac{\rho C_p}{K_T} \pm \sqrt{\left(\frac{\rho C_p}{K_T}\right)^2 + \frac{4\mu\beta}{kK_T}}\right] \quad \text{(A-11)}$$

R_1 and R_2 are integration constants. The boundary conditions are:

At the external reservoir boundary, temperature is known (geothermal temperature)

$$T\big|_{y=\frac{Y}{2}} = T_0 \quad \text{(A-12)}$$

Temperature and heat flux is continuous at the boundary between radial and linear elements

$$T\big|_{r=\frac{h}{2}} = T\big|_{y=\frac{h}{2}} \quad \text{(A-13)}$$

$$\left.\frac{dT}{dr}\right|_{r=\frac{h}{2}} = \left.\frac{dT}{dy}\right|_{y=\frac{h}{2}} \quad \text{(A-14)}$$

Heat flux is continuous at the wellbore. See Appendix B.

$$K_T \left.\frac{dT}{dr}\right|_{r=R} = U\left(T\big|_{r=R} - T_b\right) \quad \text{(A-15)}$$

This boundary condition makes the inflow temperature dependent on the wellbore temperature and the overall heat transfer coefficient between reservoir and wellbore. From the BCs, finally we have

$$L_1 = \frac{l_1 + l_2}{\psi_+ + \psi_-} \quad \text{(A-16)}$$

$$L_2 = \frac{l_3 + l_4}{\psi_+ + \psi_-} \quad \text{(A-17)}$$

$$R_1 = \frac{\theta_1 + \theta_2}{\psi_+ + \psi_-} \quad \text{(A-18)}$$

$$R_2 = \frac{\theta_3 + \theta_4}{\psi_+ + \psi_-} \quad \text{(A-19)}$$

where

$$l_1 = R^{n_-} e^{\frac{h}{2}m_-}\left(-K_T n_- + UR\right) \times \left(\beta T_o - 1\right)\left(\frac{h}{2}\right)^{n_+}\left(\frac{h}{2}m_- - n_+\right) \quad \text{(A-20)}$$

$$l_2 = \left(\frac{h}{2}\right)^{n_-}\left[e^{\frac{h}{2}m_-} R^{n_+}\left(-\frac{h}{2}m_- + n_-\right)\left(-K_T n_+ + UR\right)\left(\beta T_o - 1\right) + e^{\frac{Y}{2}m_-} UR\left(\frac{h}{2}\right)^{n_+}\left(\beta T_b - 1\right)\left(n_+ - n_-\right)\right] \quad \text{(A-21)}$$

$$l_3 = R^{n_{+3}} e^{\frac{h}{2}m_-}\left(K_T n_- - UR\right) \times \left(\beta T_o - 1\right)\left(\frac{h}{2}\right)^{n_+}\left(\frac{h}{2}m_+ + n_+\right) \quad \text{(A-22)}$$

$$l_4 = \left(\frac{h}{2}\right)^{n_-}\left[e^{\frac{h}{2}m_+} R^{n_+}\left(\frac{h}{2}m_+ - n_-\right)\left(-K_T n_+ + UR\right)\left(\beta T_o - 1\right) - e^{\frac{Y}{2}m_+} UR\left(\frac{h}{2}\right)^{n_+}\left(\beta T_b - 1\right)\left(n_+ - n_-\right)\right] \quad \text{(A-23)}$$

$$\theta_1 = e^{\frac{h}{2}(m_+ + m_-)}\frac{h}{2} R^{n_-}\left(m_+ - m_-\right)\left(K_T n_- - UR\right)\left(\beta T_o - 1\right) \quad \text{(A-24)}$$

$$\theta_2 = \left(\frac{h}{2}\right)^{n_-}\left(\beta T_b - 1\right)UR \times \left[e^{\frac{h}{2}m_+ + \frac{Y}{2}m_-}\left(\frac{h}{2}m_+ - n_-\right) + e^{\frac{Y}{2}m_+ + \frac{h}{2}m_-}\left(-\frac{h}{2}m_- + n_-\right)\right] \quad \text{(A-25)}$$

$$\theta_3 = e^{\frac{h}{2}(m_+ + m_-)} \frac{h}{2} R^{n_+} (m_+ - m_-)(-K_T n_+ + UR)(\beta T_o - 1) \quad \text{(A-26)}$$

$$\theta_4 = \left(\frac{h}{2}\right)^{n_+} (\beta T_b - 1) UR \times \left[e^{\frac{h}{2}m_- + \frac{Y}{2}m_+} \left(\frac{h}{2}m_- - n_+\right) + e^{\frac{Y}{2}m_- + \frac{h}{2}m_+} \left(-\frac{h}{2}m_+ + n_+\right) \right] \quad \text{(A-27)}$$

$$\psi_\pm = \beta R^{n_\pm} \left(\frac{h}{2}\right)^{n_\mp} (K_{Tl} n_\pm - UR) \times \left[e^{\frac{Y}{2}m_\pm + \frac{h}{2}m_\mp} \left(\frac{h}{2}m_\mp - n_\mp\right) + e^{\frac{h}{2}m_\pm + \frac{Y}{2}m_\mp} \left(-\frac{h}{2}m_\pm + n_\mp\right) \right] \quad \text{(A-28)}$$

Appendix B: Overall heat transfer

The object of this appendix is to derive the overall heat transfer coefficient used in this study. For a cased and cemented wellbore, the temperature profile near the wellbore will look like that shown in Fig. B-1. The wellbore is surrounded by casing material and cement. Fluid enters with temperature, T_I. At the inside of the cement, temperature is T_{cem} and the temperature is T_c at the inside of casing. The bulk average temperature inside the well is given as T_b. For steady state with constant thermal conductivity, the temperature distribution is given as

$$\frac{1}{r}\frac{d}{dr}\left(r\frac{dT}{dr}\right) = 0 \quad \text{(B-1)}$$

Solving this differential equation for the casing yields

$$T = T_{cem} + \frac{T_c - T_{cem}}{\ln\left(R/R_c\right)} \ln\left(r/R_c\right) \quad \text{(B-2)}$$

For the cement,

$$T = T_I + \frac{T_{cem} - T_I}{\ln\left(R_c/R_{cem}\right)} \ln\left(r/R_{cem}\right) \quad \text{(B-3)}$$

Heat flows are

$$Q_c = -2\pi R(1-\gamma)K_c \left.\frac{dT}{dr}\right|_{r=R} = 2\pi(1-\gamma)K_c \frac{T_c - T_{cem}}{\ln\left(R_c/R\right)} \quad \text{(B-4)}$$

$$Q_{cem} = -2\pi R_c(1-\gamma)K_{cem} \left.\frac{dT}{dr}\right|_{r=R_c} = 2\pi(1-\gamma)K_{cem} \frac{T_{cem} - T_I}{\ln\left(R_{cem}/R_c\right)} \quad \text{(B-5)}$$

Heat flow from wall to flowing fluid is given by

$$Q_{fl} = -2\pi R(1-\gamma)\alpha(T_c - T_b) \quad \text{(B-6)}$$

where α is a heat transfer coefficient and would be determined experimentally. From boundary layer analysis with constant wall temperature, laminar flow heat transfer coefficient is

$$\alpha = 3.656 \frac{K_{fl}}{2R} \quad \text{(B-7)}$$

For turbulent flow, Gnielinski's formula[16] is widely used. The Nusselt number is given as

$$\alpha = \frac{\left(f/2\right)(\mathrm{Re} - 1000)\mathrm{Pr}}{1 + 12.7\left(f/2\right)^{0.5}\left(\mathrm{Pr}^{2/3} - 1\right)} \frac{K_{fl}}{2R} \quad \text{(B-8)}$$

When liquid-gas two phase flow occurs, heat transfer coefficient will become flow regime dependent. Kim and Ghajar[17] presented a simple flow regime dependent correlation as

$$\alpha_{TP} = (1 - y_g)\alpha_l \left[1 + C\left(\frac{x}{1-x}\right)^m \left(\frac{y_g}{1-y_g}\right)^n \left(\frac{\mathrm{Pr}_g}{\mathrm{Pr}_l}\right)^p \left(\frac{\mu_g}{\mu_l}\right)^q \right] \quad \text{(B-9)}$$

where

$$x = \frac{\rho_g q_g}{\rho_g q_g + \rho_l q_l} \quad \text{(B-10)}$$

α_l is the liquid heat transfer coefficient and is based on the in-situ Reynolds number. The constants are given in the table below.

	C	m	n	p	q
Slug and Bubbly	2.86	0.42	0.35	0.66	-0.72
Annular	1.58	1.4	0.54	-1.93	-0.09
Stratified	27.89	3.1	-4.44	-9.65	1.56

At steady state, heat flows are equal. Then, we have

$$Q_c = Q_{cem} = Q_{fl} \equiv Q \quad \text{(B-11)}$$

Summation of the relationships gives

$$T_b - T_I = \frac{Q}{2\pi(1-\gamma)}\left[\frac{\ln\left(R_c/R\right)}{K_c} + \frac{\ln\left(R_{cem}/R_c\right)}{K_{cem}} + \frac{1}{R\alpha}\right] \tag{B-12}$$

Therefore, the overall heat transfer coefficient for the wellbore is

$$U = \frac{Q}{(T_I - T_b)2\pi R(1-\gamma)} = \left[\frac{R\ln\left(R_c/R\right)}{K_c} + \frac{R\ln\left(R_{cem}/R_c\right)}{K_{cem}} + \frac{1}{R\alpha}\right]^{-1} \tag{B-13}$$

Considering a partly opened well, the total energy entering the wellbore is then

$$\begin{aligned} -e_I\, 2\pi R_{cem} &= \left(\rho_I \hat{H}_I v_I\right)2\pi R_{cem}\gamma - q_I\, 2\pi R_{cem}(1-\gamma) \\ &= w\hat{H}_I + K_T \left.\frac{dT}{dr}\right|_{r=R_{cem}} 2\pi R_{cem}(1-\gamma) \end{aligned} \tag{B-14}$$

where w is a mass flow rate per length. Equating with the total energy from the formation is

$$-e_I\, 2\pi R = wH_I\big|_{r=R} + 2\pi R(1-\gamma)U(T_I - T_b) \tag{B-15}$$

Equating Eqs. B-14 and B-15 and considering the difference of convection term $\left(wH_I\big|_{r=R} - wH_I\big|_{r=R_{cem}}\right)$ is negligible yields

$$K_T \left.\frac{dT}{dr}\right|_{r=R_{cem}} = \frac{R}{R_{cem}}U(T_I - T_b) \tag{B-16}$$

This is the fourth boundary condition of the reservoir solution for the open hole case $\left(R/R_{cem}\ U = U\right)$.

Table 1. Parameters used for Figs. 3-5.

	Oil	*Water*	*Gas*
μ [cp]	0.6	0.5	0.017
C_p [Btu/lb °F]	0.528	1.002	0.587
ρ [lb/ft3]	43	63.027	13
β [1/°F]	0.000632	0.000311	0.00297
Permeability [md]		50	
K_{Tt} [Btu/hr ft °F]	2	2.5	1.3
Reservoir length [ft]		1000	
Reservoir width [ft]		3000	
Reservoir height [ft]		50	
T at outer boundary [^{o}F]		180	
Geothermal gradient [^{o}F/ft]		0.01	

Table 2. Well Properties

	Small	*Large*
ID [in]	2.602	4
OD [in]	3.5	4.5
Diameter with cement [in]	5	6
K_c [Btu/hr ft ^{o}F]	6.933	
K_{cem} [Btu/hr ft ^{o}F]	4.021	
Relative roughness	0.01	
Total Length [ft]	2000	
Pipe opened ratio [%]	2	

Table 3. Fluid properties

K_o [Btu/hr ft ^{o}F]	0.0797
K_g [Btu/hr ft ^{o}F]	0.0116
Salinity of water [%]	5
Specific gravity of gas	0.75
Oil API	45.176
Dissolved GOR [SCF/STB]	800
Surface tension [dyne/cm]	10
Oil Permeability [md]	50
Water Permeability [md]	50
Gas Permeability [md]	5

Table 4. Summary of wellbore results

Fluid	Rate	Diameter	ΔP_{total}	ΔT_{total}
oil	Low (5399 STB/day)	*Small*	51.5	0.5
oil	High (19742 STB/day)	*Small*	617.8	6.3
oil	Low (5164 STB/day)	*Large*	5.8	0.06
oil	High (19875 STB/day)	*Large*	81.7	0.8
gas	Low (3596 MSCF/day)	*Small*	6.3	0.2
gas	High (9986 MSCF/day)	*Small*	52.9	2.3
gas	Low (3579 MSCF/day)	*Large*	0.7	0.02
gas	High (9904 MSCF/day)	*Large*	6.2	0.3

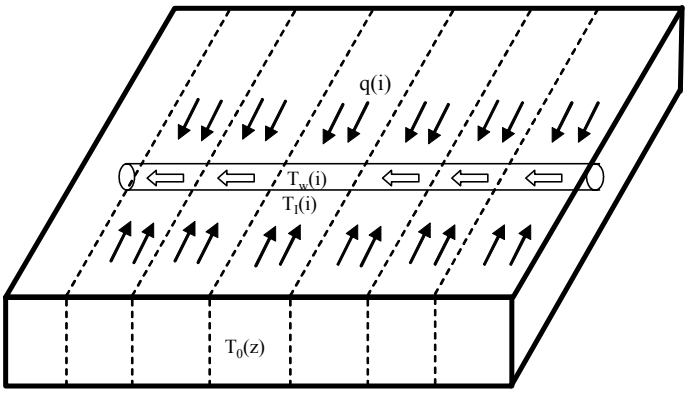

Fig. 1 Geometry of the model.

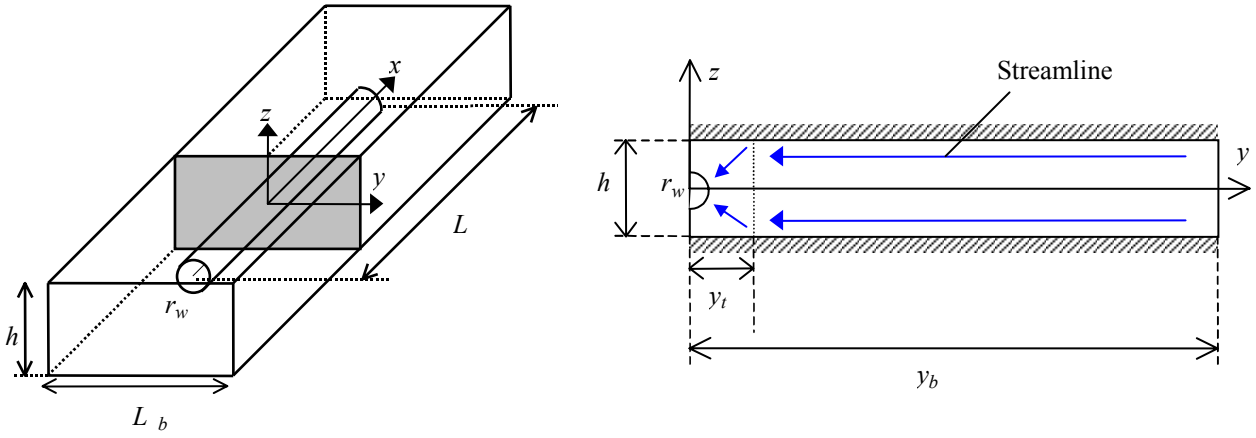

Fig. 2 Linear-radial flow geometry.

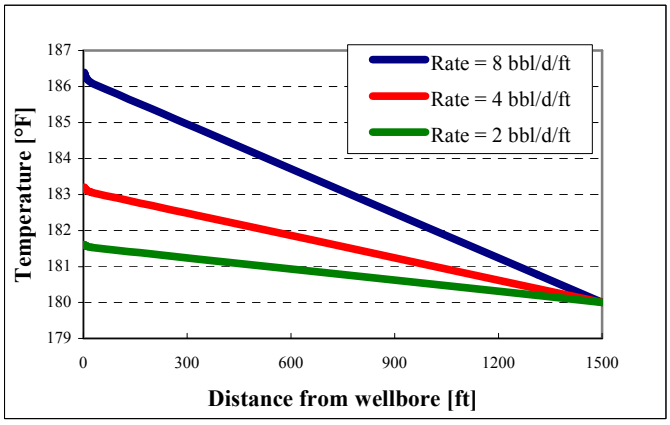

Fig. 3 Temperature profiles for different inflow rates.

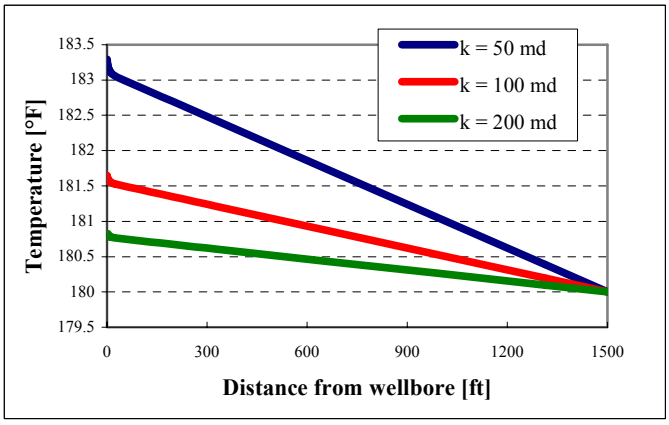

Fig. 4 Temperature profiles for different permeabilities.

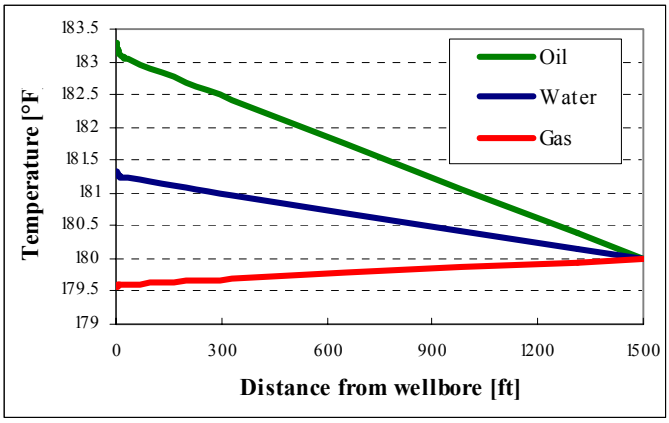

Fig. 5 Temperature profiles for different fluid types.

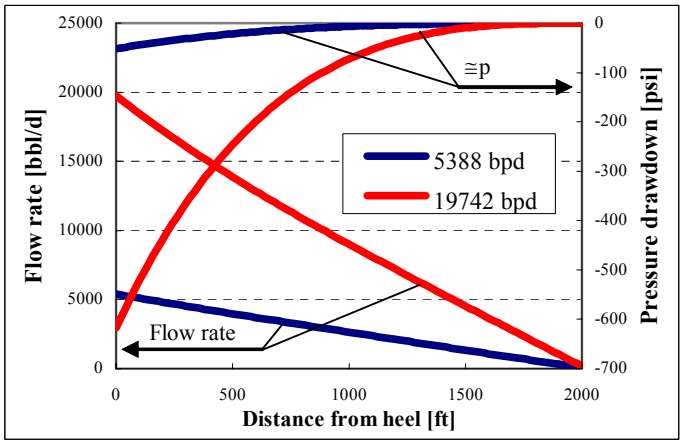

Fig. 6 Flow rate and pressure profiles (oil, small pipe).

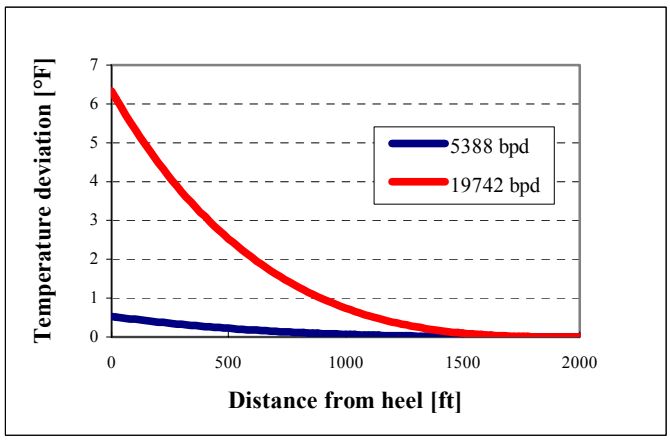

Fig. 7 Temperature profile (oil, small pipe).

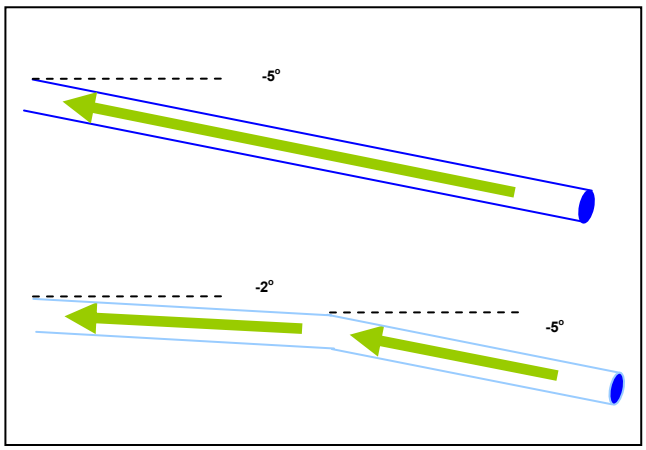

Fig. 8 Wellbore Trajectory for upwards case.

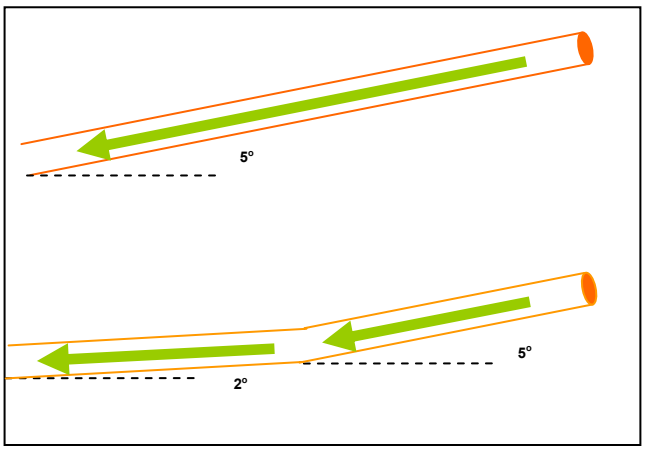

Fig. 9 Wellbore Trajectory for downwards case.

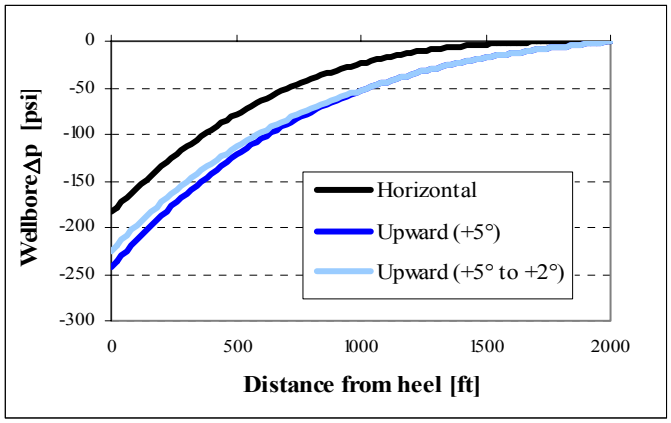

Fig. 10 Wellbore pressure drop (oil, upward).

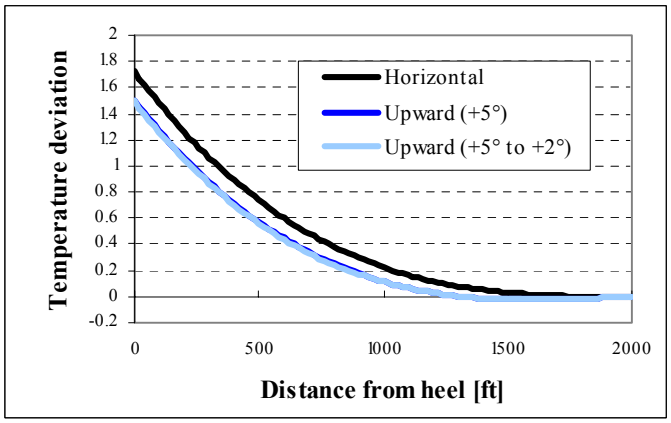

Fig. 11 Temperature deviation (oil, upward).

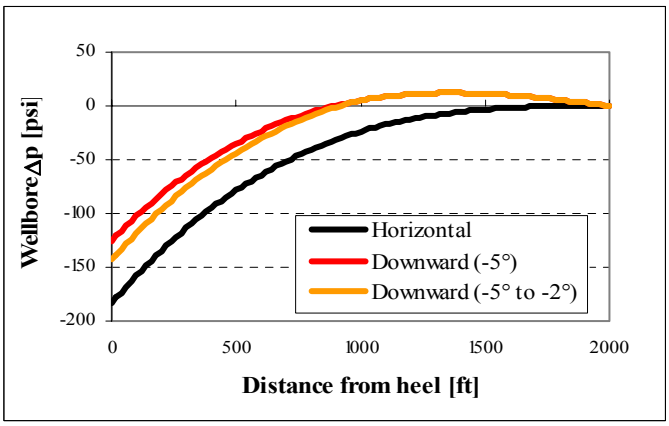

Fig. 12 Wellbore pressure drop (oil, downward).

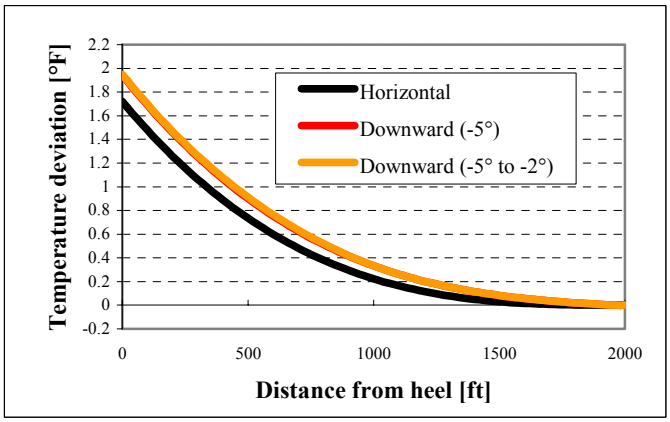

Fig. 13 Temperature deviation (oil, downward).

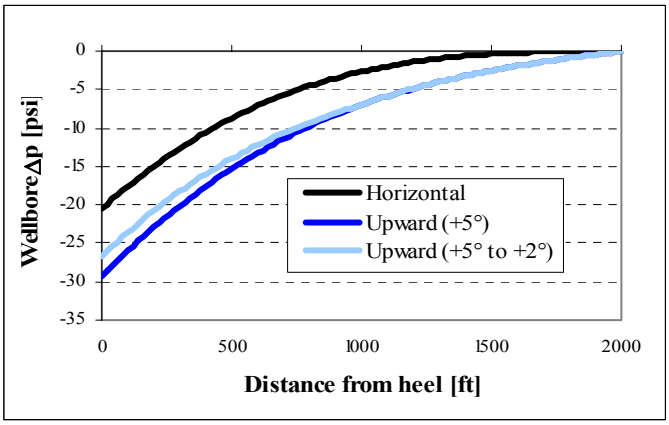

Fig. 14 Wellbore pressure drop (gas, upward).

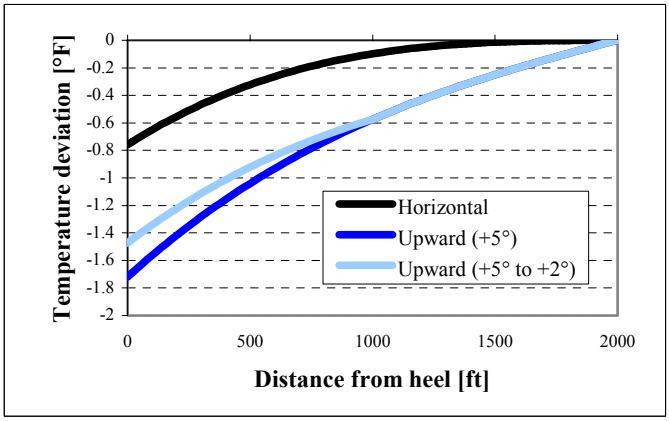

Fig. 15 Temperature deviation (gas, upward).

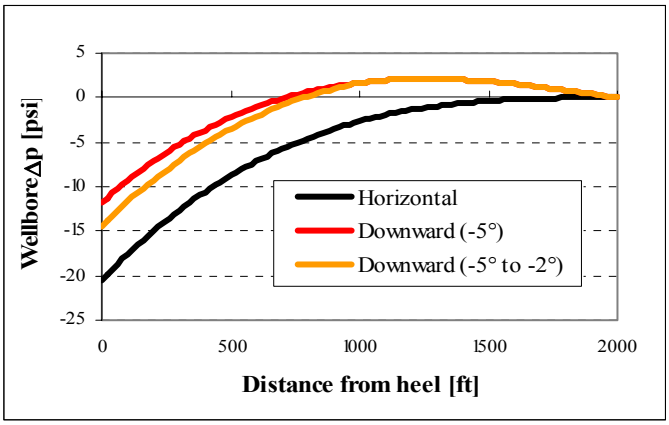

Fig. 16 Wellbore pressure drop (gas, downward).

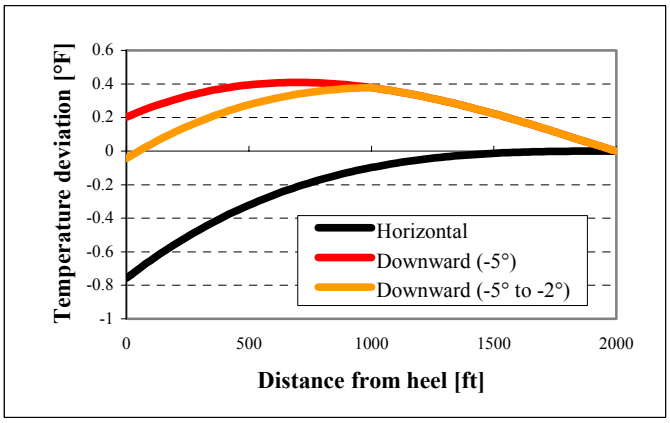

Fig. 17 Temperature deviation (gas, downward).

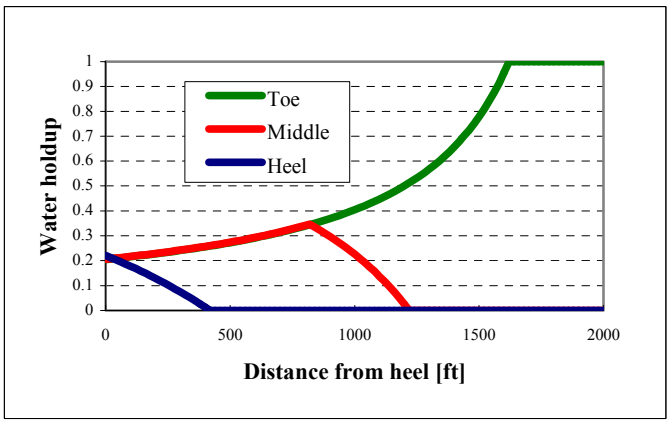

Fig. 18 Water holdup profiles (water entry).

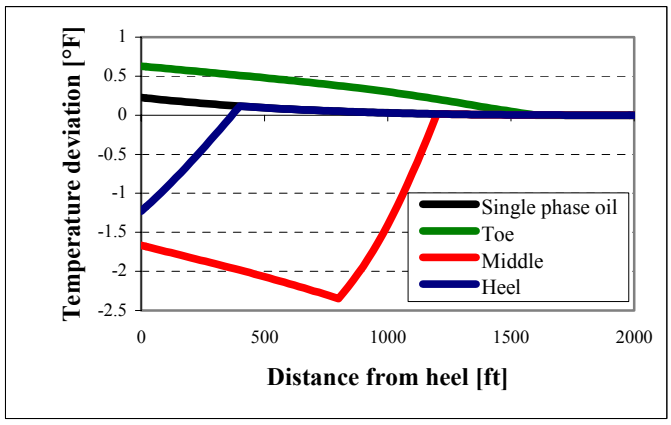

Fig. 19 Temperature deviation profiles (water entry).

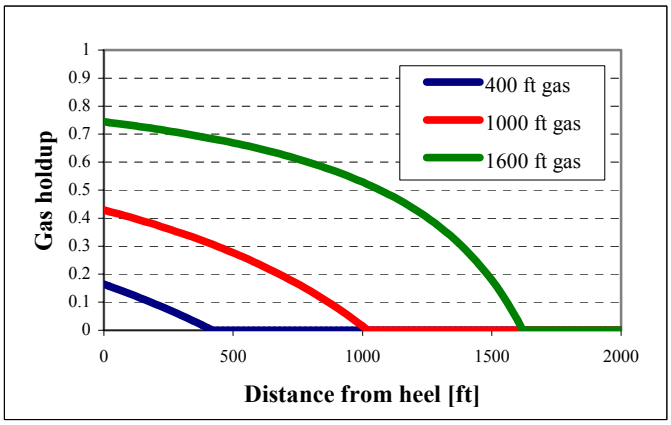

Fig. 20 Gas flow rate and holdup profiles (oil-gas).

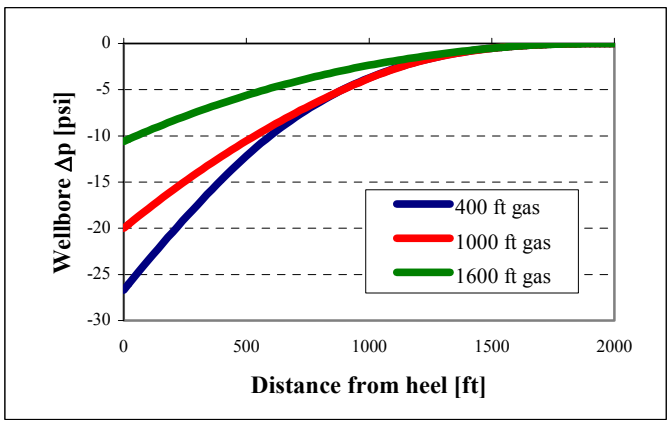

Fig. 21 Pressure drawdown profiles (oil-gas).

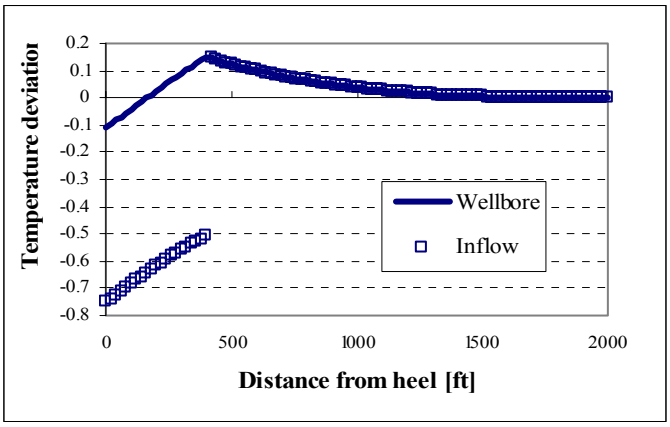

Fig. 22 Temperature deviation profile (400 ft gas).

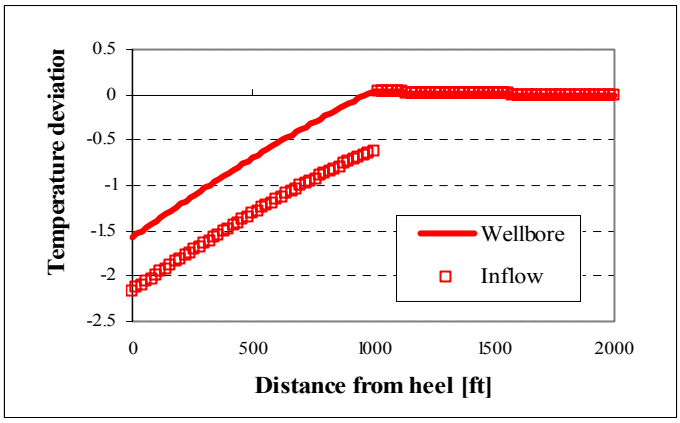

Fig. 23 Temperature deviation profile (1000 ft gas).

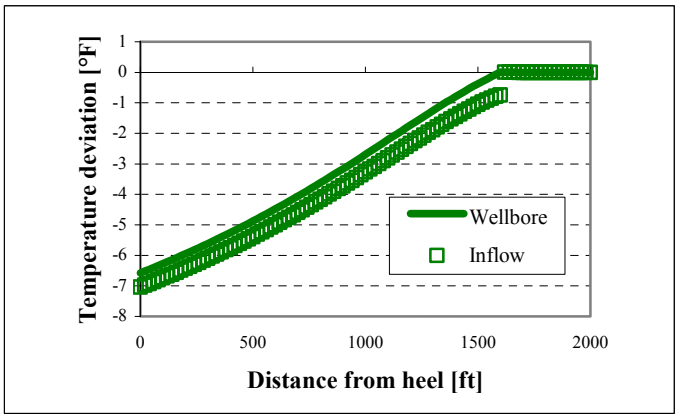

Fig. 24 Temperature deviation profile (400 ft gas).

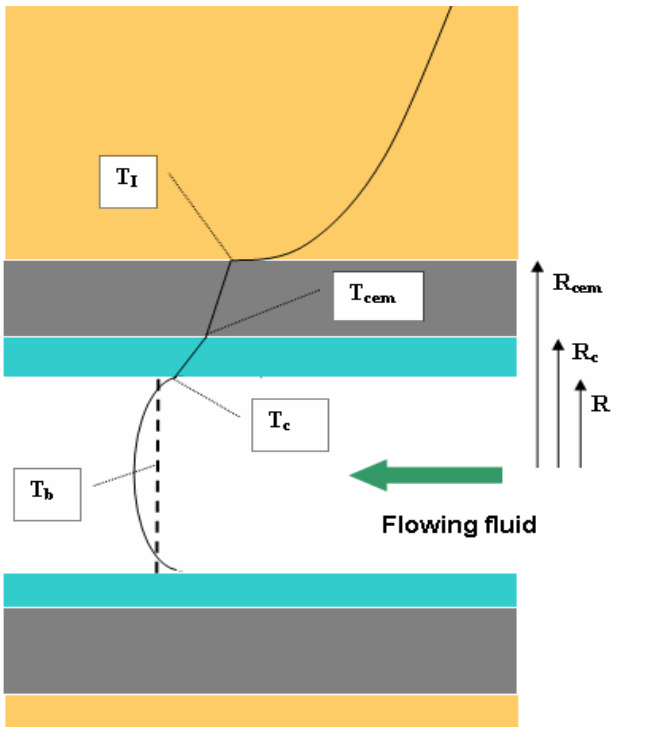

Fig. B-1—Temperature profile near wellbore.